B. XU, H. FU, Q. H. XIAO, S.LI, T. KANG

ISSN 0543-5846
METABK 59(2) 156-158 (2020)
UDC – UDK 669.15/621-41:621.791.052:531.79:620.16=111

NUMERICAL SIMULATION OF THE INFLUENCE OF WELDING DIRECTION ON RESIDUAL STRESS AFTER DOUBLE WELDING OF Q345 STACKED-PLATES

Received – Primljeno: 2019-08-28
Accepted – Prihvaćeno: 2019-10-25
Original Scientific Paper – Izvorni znanstveni rad

Based on the welding numerical simulation software Visual-environment, this paper calculates and analyzes the residual stress field for the double pass welding of Q345 stacked plates. The paper mainly studies the influence of different welding directions on the residual stress after welding. The results show that different welding methods have little effect on the lateral residual stress, while the longitudinal residual stress and the initial and end of the weld have a greater influence, while the post-weld residual stress distribution of the anisotropic two-pass weld is more uniform.

Keywords: double weld, numerical simulation, anisotropic, residual stress

INTRODUCTION

During the welding process, due to the concentrated energy of the welding heat source, the heat distribution on the entire work piece during the welding process is uneven, and the uneven heat distribution causes the work piece stress to change [1-3]. The stress of welding consists of the instantaneous stress generated during the welding process and the residual stress after the complete cooling after welding, resulting in uneven distribution of the residual stress of the whole work piece after welding, and the residual stress will affect the working strength of the welded component to some extent [4-7]. In the two-pass welding of the plate, the same direction welding and the anisotropic welding have different effects on the temperature field of the work piece and the distribution of residual stress after welding [8]. Therefore, it is very important to grasp the different welding directions of the plates for the residual stress distribution after welding [9-11]. With the development of simulation technology, the numerical simulation of welding residual stress has become one of the main hotspots in the current research [12-15].

In this paper, the numerical simulation of the welding process of double-plate double-pass welding is carried out, and the simulation of double-pass welding is simulated by using Visual-environment combined with sysweld finite element software. Predict the residual stress distribution after welding in the case of different welding directions in the second pass, which provides a theoretical basis for practical work.

Yurianto, S. H. Suryo, Y. Umardani, Mechanical Engineering Department, Diponegoro University, Semarang, Indonesia. Corresponding author: yurianto_narimin@yahoo.com

Experiment process

In this paper, the model-meshing software visual-mesh in visual-environment is used to establish the model and mesh, and the pre-processing setting and calculation are performed by visual-weld. The calculation model is set to two plates of 200 mm × 50 mm × 4 mm by visual-mesh. The width of the stack is 5mm. The welding seam above the plate 1 is the first welding seam, and the welding seam under the plate 2 is the second, and the cross section is shown in Figure 1. The meshing method adopts Topo adaptive meshing, and linear mesh distribution is used in the horizontal direction of the two plates, so that the area mesh close to the welding seam is denser and the calculation accuracy is improved. The material of the plate and the weld is Q345, and the composition is shown in Table 1.

Table1 **Chemical composition of Q345 steel/ wt, %**

C	Mn	Si	S	P
0,20	1,60	0,55	0,035	0,035

Table 2 **Experiment scheme**

	Amp/A	Vol / V	Line power / (J / mm)	Direction of 2nd pass
Case1	27	15	288	- y
Case2	27	15	288	+ y

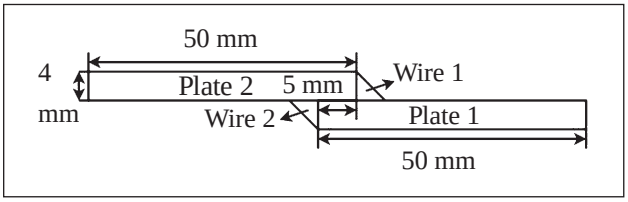

Figure 1 Welding model

The experimental scheme of this paper mainly considers the influence of the direction of the second welding on the final residual stress distribution of the double pass welding. Therefore, the direction of the second welding is the main variable of the simulation experiment, and the welding direction of the first pass is + y direction. The heat source model in the simulation process adopts a double ellipsoid model which is more in line with the actual welding conditions. The experimental scheme is shown in Table 2, and the speed of weld is 10mm/s.

The welding process during arcing involves the processes of heat conduction, convection, radiation, evaporation and melting and solidification, including many complex physical and chemical metallurgical processes. Therefore, the following assumptions are made during the numerical simulation:

a) Assume that surface deformation does not change heat transfer and mass transfer between the welding arc and the work piece;
b) Ignore the fuzzy area where the solid-liquid two phases coexist in the molten pool.

Simulation results and analysis

Figure 2 (a) and (b) shows the final residual stress distribution cloud map for two different cases. Through observation, the residual stress distribution characteristics of the edge regions of the lower plates of different schemes are similar. The residual stress difference between the two ends of the welding seam and the middle position is large, especially at the beginning and end of the first weld. The points of the point of the residual stress maximum and the minimum value of the work piece are close to each other on the plate, and the maximum worth points are distributed in the middle of the weld, and the minimum points are at the corners of the work piece. It can be seen that different welding directions have a greater influence on the final residual stress distribution.

Figure 3 (a) and (b) shows the transverse (x - direction) residual stress distribution curves of the two plates in both cases, with the selected position at the lateral

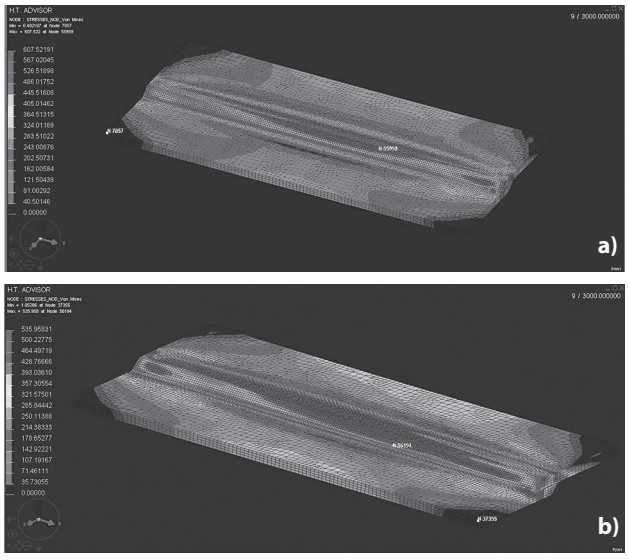

Figure 2 Residual stress distribution cloud diagram after welding ends to room temperature in two cases. (a) case1; (b) case2.

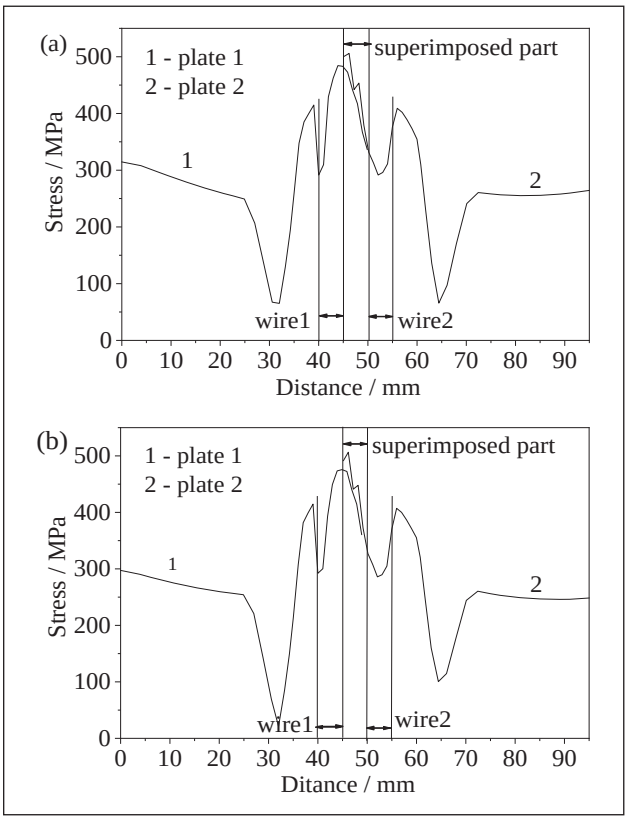

Figure 3 Lateral residual stress distribution in two cases

centerline of the plate. It can be seen from the comparison that the residual stress distribution of the anisotropic welding and the co-directional welding is substantially the same, and the residual stresses of the stacked positions of the two plates are the highest and both are close to the first weld, which is because the temperature gradient is larger when the first pass of the welding heat source passes, and the temperature gradient of the second pass is smaller than the first pass. The maximum residual stress of the counter-welded plate 1 is 484,37 MPa, the plate 2 is 505,82 MPa, the co-welded plate 1 is 475,73 MPa, and the plate 2 is 506,44 MPa, what can be seen that the two cases have little effect on the residual stress distribution at the lateral centerline position of the plate. At the same time, the residual stress of the weld is closer to the residual stress in the stacking area, and the residual stress in the heat-affected zone is significantly higher than the edge of the weld, the residual stress at the edge of the heat-affected zone decreases first and then increases to the edge of the plate, which is because the temperature change in the heat affected zone at 30 mm is more gradual than in other locations. It can be seen from the above that the difference in the welding direction has little effect on the distribution of the lateral residual stress of the plate.

Figure 4 is the longitudinal (+ y - direction) residual stress distribution curve of the heat affected zone of the two plates in two cases, and the direction of the selection is consistent with the welding direction of the pass. It can be seen from the comparison that the residual stress is basically the same in the middle of the plate. However, there is a big gap between the initial and the arc end of the welding, that is, the residual stress distribution after the

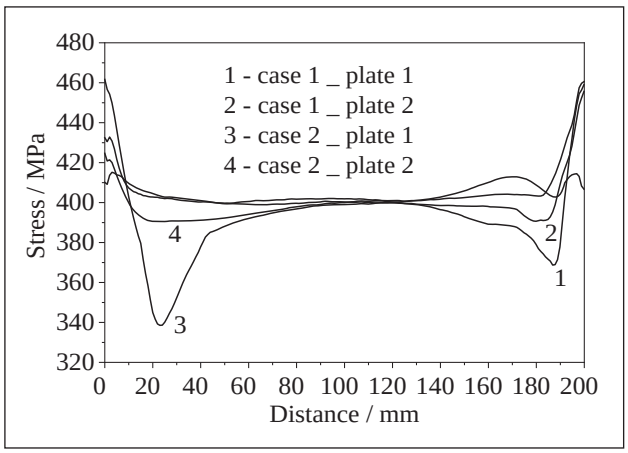

Figure 4 vertical residual stress distributions in two cases

heat source starts and acts at each pass, which is caused by the arc being unstable in arcing and arcing, and the instability of the arc causes uneven stress distribution at the beginning and end of the welding. Comparing the residual stress of the plate 1 in the two cases, it can be seen that the residual stress at the starting end is 461,68 MPa, which is 12,56 % larger than the anisotropic welding, because the welding start positions of the two passes of the same direction welding are the same. Also, since the direction of the second pass of the counter-welding is opposite to the direction of the first pass, the residual stress of the counter-welded plate 1 at the end is 455,05 MPa, which is 12,87 % larger than that of the co-weld. Comparing the residual stress of the plate 2, it is found that the residual stress distribution is not much different. In addition, the residual stress distribution of the two cases can be seen that the residual stress distribution of the anisotropic welding is more uniform than that of the same direction welding. Therefore, in the actual welding process, the two pase welding of the sheet should be performed by the opposite direction

SUMMARY

For the anisotropic two-pass welding and the same-direction two-pass welding, the residual stress is mainly concentrated in the weld area, and the maximum temperature residual stress due to the first pass is near the first weld, the point where the residual stress is the smallest is distributed at the corners.

For the anisotropic two-pass welding and the same-direction two-pass welding, the direction of the second pass welding has little effect on the lateral residual stress. However, in the longitudinal residual stress, the welding direction has a greater influence on the residual stress distribution at the end. By comparing the overall residual stress distribution, it can be concluded that the residual stress distribution of the anisotropic two-pass welding is more uniform, and the welding method of the anisotropic two-pass welding should be adopted in the actual welding.

Acknowledgments

This work was financially supported by Opening Fund for National Key Laboratory of Metallic Materials for Marine Equipment and Application (SKLMEA-K201801), Liaoning Province Natural Science Fund Project (201602385), 2017 Provincial Key Laboratory Opening Project of Liaoning University of Science and Technology (USTLKFSY201709), Liaoning Provincial Department of Education Innovation Team Project (LT2016003).

REFERENCES

[1] V. M. V. Prasad, V. M. J. Varghese, M. R. Suresh, et al. 3D simulation of residual stress developed during TIG welding of stainless steel pipes [J], Procedia Technology 24 (2016), 364 - 371.

[2] J. Tomków, G. Rogalski, D. Fydrych. Improvement of S355G10+N steel weldability in water environment by Temper Bead Welding [J], Journal of Materials Processing Tech 262 (2018), 372 - 381.

[3] F. S. Neto, D. Neves, O. M. M. Silva, et al. An Analysis of the Mechanical Behavior of AISI 4130 Steel after TIG and Laser welding process [J], Procedia Engineering 114 (2015), 181 - 188.

[4] N. Sayyar, M. Shamanian, B. Niroumand. Arc weldability of Incoloy 825 to AISI 321 stainless steel welds [J], Journal of Materials Processing Tech 262 (2018), 562 - 570.

[5] Z. Ye, J.H. Huang, Z Cheng, et al. Combined effects of MIG and TIG arcs on weld appearance and interface properties in Al/steel double-sided butt welding-brazing [J], Journal of Materials Processing Tech 250 (2017), 25 - 34.

[6] H. M. Soltani, M. Tayebi. Comparative study of AISI 304L to AISI 316L stainless steels joints by TIG and Nd: YAG laser welding [J], Journal of Alloys and Compounds 767 (2018), 112 - 121.

[7] R. Bendikiene, S. Baskutis, J. Baskutiene, et al. Comparative study of TIG welded commercially pure titanium [J], Journal of Manufacturing Processes 36 (2018), 155 - 163.

[8] B. Wu, B. Wang, X. T. Zhao, et al. Effect of active fluxes on thermophysical properties of 309L stainless-steel welds [J], Journal of Materials Processing Tech 255 (2018), 212 - 218.

[9] X. G. Li, B. M. Gong, C. Y. Deng, et al. Effect of pre-strain on microstructure and hydrogen embrittlement of K-TIG welded austenitic stainless steel [J],Corrosion Science 149 (2019), 1-17.

[10] K.H. Teng, Y. J. Shi. Effect of thermal stability of powdered oxide on joint penetration and metallurgical feature of AISI 4130 steel TIG weldment [J], Powder Technology 286 (2015), 31 - 38.

[11] K. L. Wu, X. J. Yuan, T. Lia, et al. Effect of ultrasonic vibration on TIG welding–brazing joining of aluminum alloy to steel [J], Journal of Materials Processing Tech 266 (2019), 230 - 238.

[12] M. A. Derakhshi, J. Kangazian, M. Shamanian. Electron beam welding of inconel 617 to AISI 310: Corrosion behavior of weld metal [J], Vacuum 161 (2019), 371 - 374.

[13] G. D. Q. Caetano, C. C. Silva, M. F. Motta, et al. Influence of rotation speed and axial force on the friction stir welding of AISI 410S ferritic stainless steel [J], Journal of Materials Processing Tech 262 (2018), 430 - 436.

[14] Y. F. Zhang, J. H. Huang, Z. Cheng, et al. Study on MIG-TIG double-sided arc welding-brazing of aluminum and stainless steel [J], Materials Letters 172 (2016), 146 - 148.

[15] M. Aissani, S. Guessasma, A. Zitouni, et al. Three-dimensional simulation of 304L steel TIG welding process: Contribution of the thermal flux [J], Applied Thermal Engineering 89 (2015), 822 - 832.

Note: Q.H.XIAO is responsible for English language, Liaoning, China